J Mater Sci: Mater Electron

Study of structural and luminescent characteristics of novel color tunable blue-green Tb^{3+}-doped $Na_3Y(PO_4)_2$ nanoparticles for NUV-based WLEDs

Manju Dahiya[1], Anju Siwach[1], Mandeep Dalal[2], and Dinesh Kumar[1,*]

[1] Department of Chemistry, Deenbandhu Chhotu Ram University of Science and Technology, Murthal, Sonepat 131039, India
[2] Department of Chemistry, Maharshi Dayanand University, Rohtak 124001, India

Received: 19 October 2020
Accepted: 21 December 2020

ABSTRACT

Nanoscaled Tb^{3+}-doped $Na_3Y(PO_4)_2$ phosphors with magnificent color domain have been synthesized via urea-assisted solution combustion process and characterized by powder X-ray diffraction (XRD), transmission electron microscopy (TEM), energy-dispersive X-ray spectroscopy (EDX), and photoluminescence (PL) studies. The Rietveld refinement was executed on the XRD data of $Na_3Y_{0.96}Tb_{0.04}(PO_4)_2$ and showed that the samples were crystallized into a single-phase orthorhombic lattice with space group Pca21(29). Additionally, TEM micrograph, and Debye–Scherrer equation analysis of $Na_3Y_{0.96}Tb_{0.04}(PO_4)_2$ revealed the occurrence of nanosized phosphor particles in a size domain lying between 25 and 40 nm. Furthermore, to forecast PL of the as-synthesized nanophosphors, their PL emission and excitation spectra were recorded at a wavelength of 374 and 545 nm, respectively. Under the excitation wavelength (at λ_{ex} = 374 nm), the PL emission spectra of $Na_3Y_{(1-x)}Tb_x(PO_4)_2$ (where x = 0.015–0.06 mol) exhibited the appearance of most intense peak at 545 nm corresponding to $^5D_4 \rightarrow {}^7F_5$ (magnetic dipole allowed) transition. Critical concentration for the nanophosphors series was found to be x = 0.04 (4 mol%) and also the critical transfer distance (R_c) was determined to be 21 Å which ultimately depicted the energy transfer mechanism majorly responsible for concentration quenching as quadrupole–quadrupole interactions. Quantum efficiency for the whole series was calculated and intrinsic lifetime (4.03 ms) was also determined using Auzel's fitting parameters. CIE coordinates (x, y) for series $Na_3Y_{1-x}Tb_x(PO_4)_2$ (where x = 0.015–0.05 mol) were also evaluated by MATLAB software and their results showed that the color tunability from bluish to greenish can be achieved simply by changing the concentration of dopant ions. All the as-obtained results suggest that $Na_3Y_{1-x}(PO_4)_2{:}xTb^{3+}$ nanophosphors may show their potential usability as a blue-green component in Near-Ultraviolet (NUV)-based WLEDs, and display gadgets.

Address correspondence to E-mail: dineshdalal8@rediffmail.com

https://doi.org/10.1007/s10854-020-05158-w
Published online: 11 January 2021

1 Introduction

Over recent years, nanophosphors have shown various potential applications such as field emission, solid-state laser devices, solar cells, and white light-emitting diode (WLEDs) [1, 2]. Researchers are giving more attention in the search for these nanomaterials because of their properties work in different ways at the nanoscale as compared to that of the bulk level [3]. WLEDs have replaced the conventional lighting devices such as incandescent bulbs and compact fluorescent lamps (CFLs) because WLEDs have many advantages such as low energy consumption, high luminescent efficacy, long service time, eco-friendly and relatively small size [4–6]. In the past few years, GaN blue-LED chips (λ_{ex} = 450–470 nm) coated with yellow-emitting YAG: Ce^{3+} phosphor were utilized to fabricate WLEDs. Later on, due to the appearance of certain limiting factors such as poor color rendering index and high correlated color temperature, these WLEDs have been restricted to white light emission [7–12]. To nullify the drawbacks of the earlier methods, the main objective to develop WLEDs of the new era is attained either using near-ultraviolet (NUV) LED chips (λ_{ex} = 350–420 nm) covered with tricolor red, green, and blue (RGB) phosphors or blue-LED coated with red or green phosphors to solve the problem of poor color rendering index and high correlated color temperature [13–15]. Therefore, the WLEDs developed in this manner show small power utilization, longer lifetime, cost reduction as well as color tunability at different concentrations [16–18]. The capacity and strength of RGB phosphor-based WLEDs depend upon the nature of red, green and blue phosphors materials [19]. Consequently, the fabrication of a stable and potent green-emitting phosphor with the NUV excitation region is very purposeful.

Nanophosphors are synthesized by doping of activator ion, i.e., a lanthanide or transition ion into a host matrix [20]. Luminescent properties of a phosphor depend upon activator ions which are incorporated into the host lattice [21]. Furthermore, Tb^{3+} ion is considered one of the most important dopants among different rare-earth ions for green luminescence with the NUV excitation regions [22, 23]. Also, the selection of host matrix along with activator ions is a matter of consideration. However, various Tb^{3+} activated phosphors have been fabricated using different host matrix such as aluminates [1], borates [2, 24], nitrides [25], tungstate [26], and phosphates [27, 28]. But at present, phosphate-based host series have many advantages such as less sintering temperature, low cost of synthesis, and high chemical stability. By keeping in mind the above advantages of phosphate-based host matrix, the author has selected $Na_3Y(PO_4)_2$ (NYPO) as the inorganic host matrix that belongs to the family of double phosphates of monovalent cations (like Na^+ or K^+ ions). The structural properties of NYPO were investigated by Aleksandra Matraszeket et al. [29]. The main building blocks in NYPO host are PO_4 tetrahedral units which share their oxygen ions with ReO_8 polyhedral units. $Na_3Y(PO_4)_2$ exhibits structural phases transitions such as trigonal, orthorhombic and monoclinic lattice which further depends upon the method of synthesis adopted and sintering temperature [29].

To the best of author's knowledge, there is no report on the synthesis, structural and optical properties of Tb^{3+}-doped $Na_3Y(PO_4)_2$ nanophosphor by any method published so far. So, in this research, the author made an attempt to synthesize a series of novel green-emitting, single-phase $Na_3Y_{1-x}(PO_4)_2$: xTb^{3+} (where x = 0.015–0.06 mol) via urea-assisted solution combustion method which is suitable for use in NUV-based WLEDs as its excitation wavelength 374 nm fits well with characteristics emission of NUV LED chips. The solution combustion method has many practical advantages such as the lower-temperature requirement, less time consumption, low temperature and produces a homogenous product [30, 31]. XRD analysis was used to examine the purity of fabricated samples. Structural and morphological properties were studied with the help of Rietveld refinement analysis, and TEM techniques, while photoluminescent properties were investigated to determine the emission and excitation region. Furthermore, Quantum efficiency, radiative rates and non-radiative rates were found for the whole series with the help of the PL decay curve. At last, CIE coordinates for the series of $Na_3Y_{(1-x)}Tb_x(PO_4)_2$ (where x = 0.015–0.05 mol) were also calculated to determine the emitted color. All the results showed that obtained nanophosphors have practical applicability for RGB phosphor-based WLEDs in NUV region and for other light-emitting devices.

2 Experimental

2.1 Materials and synthesis

A sequence of $Na_3Y_{1-x}(PO_4)_2{:}xTb^{3+}$ (where x = 0.015, 0.025, 0.035, 0.04, 0.05, and 0.06 mol) phosphors was synthesized via urea-assisted solution combustion method. The raw materials used for synthesis of phosphors were sodium nitrate ($NaNO_3$) (A.R), yttrium nitrate hexahydrate ($Y(NO_3)_3.6H_2O$) (99.9%), terbium nitrate hexahydrate ($Tb(NO_3)_3.6H_2O$) (99.9%), diammonium hydrogen phosphate ($(NH_4)_2HPO_4$) (A.R), and urea (NH_2CONH_2) (A.R) were purchased from Sigma Aldrich. Their stoichiometric amounts were dissolved in the minimum amount of double-distilled water into a 500 ml beaker. The stoichiometric quantity of fuel, i.e., urea was calculated according to oxidizing and reducing valency of oxidizer and fuel. The mixture was concentrated by heating on a hot plate until the excess of water get evaporated and the concentrated solution was then transferred into a preheated muffle furnace maintained at 500°C for 10–15 minutes. In the beginning, the solution went through rapid dehydration followed by the liberation of an enormous amount of gaseous by-products such as the oxides of carbon and nitrogen. These volatile gases burnt with a glow producing bulky solid. Afterward, this solid was crushed using a mortar pestle to attain pulverized form which was further calcined at 1100°C for 3 hours. The general exothermic combustion reaction occurred during the synthesis of $Na_3Y_{0.96}Tb_{0.04}(PO_4)_2$ phosphor is given below:

$$75NaNO_3 + 24Y(NO_3)_3.6(H_2O) + Tb(NO_3)_3.6(H_2O) + 50(NH_4)_2H(PO_4) + 600NH_2CONH_2 \rightarrow 25Na_3Y_{0.96}Tb_{0.04}(PO_4)_2 + 725N_2 + 600CO_2 + 1575H_2$$

2.2 Characterization techniques

The crystal phase of $Na_3Y(PO_4)_2$: Tb^{3+} phosphor was confirmed by a high-resolution Rigaku Ultima-IV X-ray diffractometer having Cu K_α radiations source operating at 40 kV and 40 mA voltage and tube current, respectively. The samples were scanned in a 2θ range of 10° to 60° at a constant scanning rate 2° per minute. The qualitative and quantitative studies of sample $Na_3Y_{0.96}Tb_{0.04}(PO_4)_2$ calcined at 1100°C were examined using the Rietveld refinement technique. The grain size of particles and morphology were studied by the Technai G^2 FEI transmission electron microscope (TEM). Hitachi F-7000 fluorescence spectrophotometer fitted with Xe lamp as the excitation source of light was used to study the optical properties of nanophosphors. The slit width that we used to study luminescent properties was set at 2.5 nm. The voltage of the photomultiplier tube was also set at 400 V. All the investigations were performed at room temperature.

3 Results and discussion

3.1 Structural analysis

XRD pattern of the as-synthesized $Na_3Y_{(1-x)}Tb_x(PO_4)_2$ (where x = 0.015, 0.025, 0.035, 0.04, 0.05, and 0.06 mol) phosphors along with standard JCPDS data is shown in Fig. 1. It can be shown from the X-ray diffractogram that all the XRD peaks match well with JCPDS data of the host with some minor impurities appeared at about 2θ = 31.8 which further concludes that the activator Tb^{3+} ions are doped homogenously in host $Na_3Y(PO_4)_2$ lattice without any structure modifications. Figure 2 portrays the Rietveld refinement of $Na_3Y_{0.96}Tb_{0.04}(PO_4)_2$ where the solid red line represents the calculated diffraction pattern and the observed diffraction profile is shown by a black diamond. The difference between calculated and observed diffraction patterns is shown by the blue

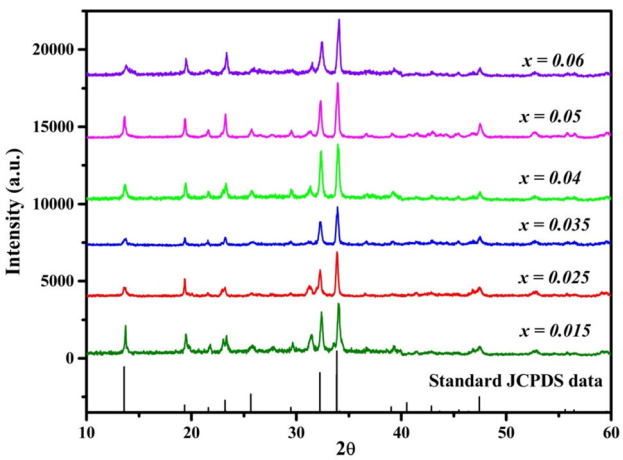

Fig. 1 XRD profile of $Na_3Y_{(1-x)}Tb_x(PO_4)_2$ (x = 0.015–0.06 mol) nanophosphors along with JCPDS data of $Na_3Y(PO_4)$

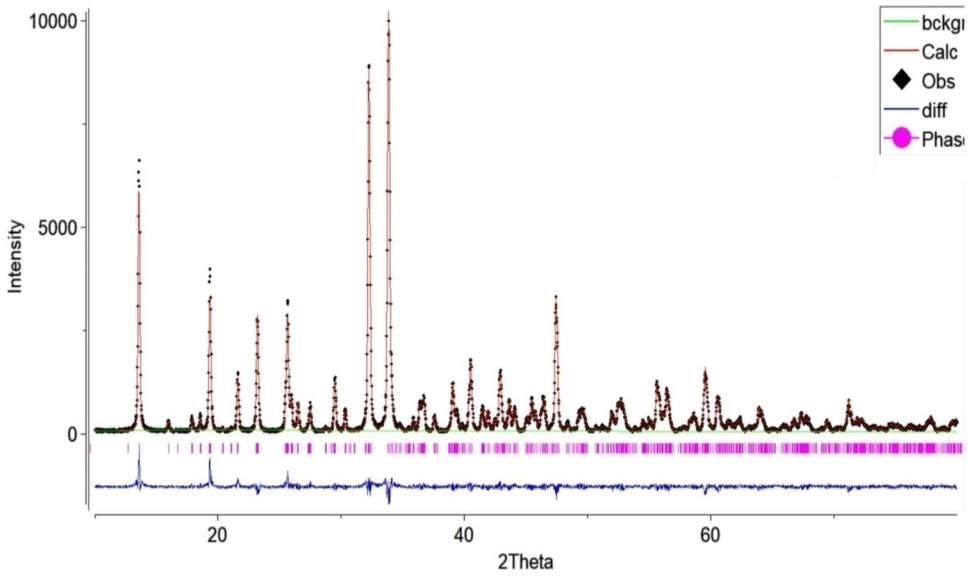

Fig. 2 Rietveld refinement of $Na_3Y_{0.96}Tb_{0.04}(PO_4)_2$ nanophosphor with refinement parameters $\chi^2 = 4.71$, $R_{wp}(\%) = 11.32$, and $R_p(\%) = 8.45$

line which is lying just above X-axis. Lattice parameters determined by the Rietveld refinement are as $a = 13.9447$ Å, $b = 5.2994$ Å, $c = 18.3310$ Å and $\alpha = \beta = \gamma = 90$, V = 1354.63Å^3, and Z = 8. The Rietveld refinement of $Na_3Y_{0.96}Tb_{0.04}(PO_4)_2$ phosphor confirms that crystal structure is orthorhombic with space group Pca21(29). The comparison of crystal lattice data of $Na_3Y_{0.96}Tb_{0.04}(PO_4)_2$ phosphor with the standard data of host [29] is shown in Table 1. The complete crystal structure of $Na_3Y_{0.96}Tb_{0.04}(PO_4)_2$ and the coordination environment around different cations are depicted in Fig. 3. The structural analysis further reveals the occurrence of six types of Na^+ ions sites and two Y^{3+}/Tb^{3+} ions sites which are found in six and eight coordinated irregulars polyhedral units, respectively. P^{5+} ions are four-coordinated tetrahedral which shares its oxygen with ReO_8 (Re = Y^{3+}/Tb^{3+}) polyhedral.

Furthermore, the radius percentage difference during replacement of Y^{3+} ions by Tb^{3+} is calculated by the equation given below [32]:

$$\Delta_r = \frac{(CN)R_{m\_} - R_d(CN)}{R_m(CN)} \times 100 \quad (1)$$

where R_m stands for ion radius of the host, R_d shows ionic radii of dopant ion and CN represents coordination number. The value of radius percentage difference comes out to be 1.7% which is not exceeding the acceptable value, i.e., 30% and thereby, it confirms the substitution of Y^{3+} ions by Tb^{3+} ions without any disturbance.

The average crystallite size $Na_3Y_{(1-x)}Tb_x(PO_4)_2$ (where $x = 0.015$–0.06 mol) is determined by a well known the Debye–Scherer's equation [33–35]:

Table 1 Comparison of crystal structure parameters of $Na_3Y_{0.96}Tb_{0.04}(PO_4)_2$ nanophosphor system with $Na_3Y(PO_4)_2$ host lattice

Formula	$Na_3Y(PO_4)_2$	$Na_3Y_{0.96}Tb_{0.04}(PO_4)_2$
Formula weight (g/mol)	347.82	350.62
Crystal shape	Orthorhombic	Orthorhombic
Space group	Pca21 (29)	Pca21 (29)
a (Å)	13.94	13.9447 (15)
b (Å)	5.292	5.2994 (8)
c (Å)	18.33	18.3310 (28)
α (degree)	90	90
β (degree)	90	90
γ (degree)	90	90
Volume (Å^3)	–	1354.63 (18)

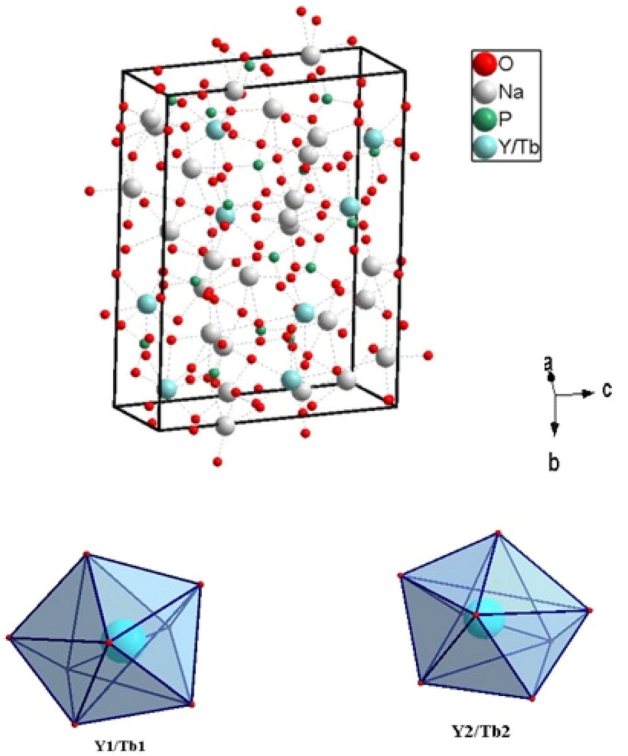

Fig. 3 Crystal lattices view of $Na_3Y_{0.96}Tb_{0.04}(PO_4)_2$ nanophosphor along with the coordination environment of different cations

$$D = \frac{0.941\lambda}{\sqrt{\{\beta_o^2(2\theta) - \beta_{si}^2(2\theta)\}}\cos\theta} \quad (2)$$

where D represents average crystallite size, λ is X-ray wavelength (0.15406 nm), θ is diffraction angle and $(\beta_o(2\theta))$ and $(\beta_{si}(2\theta))$ stand for observed and standard full width at half maximum for silicon pattern (FWHM), respectively. From the Scherrer equation, the crystallite size comes out to be 25–35 nm. The strain (ε) and dislocation density (δ) are also determined using the following equations, respectively [36]:

$$\epsilon = \frac{\beta cos\theta}{4} \quad (3)$$

The results thus obtained from the above-mentioned equations are tabulated in Table 2.

$$\delta = \frac{1}{D^2} \quad (4)$$

3.2 Morphological studies

Surface morphological properties and grain size of synthesized NYPO:Tb^{3+} samples are obtained by TEM analysis. Figure 4 represents the TEM micrograph of $Na_3Y_{0.96}Tb_{0.04}(PO_4)_2$ phosphor calcined at 1100°C. After analysis of micrograph, author reveals that a grain size of samples lies in range of 25–40 nm, which is also confirmed by Debye–Scherrer's equation. At nanoscale, these phosphors have large surface to volume ratio and less internal scattering as compared to bulk system, resulting in the intensification of photoluminescent properties with lesser non-radiative emission [37].

Furthermore, the energy-dispersive X-ray (EDX) spectroscopy tool is used to confirm the elemental constituents of a chemical compound containing more than one element. EDX analysis confirms the presence of sodium, phosphorus, yttrium, oxygen, and terbium elements in $Na_3Y_{0.96}Tb_{0.04}(PO_4)_2$ which is shown in Fig. 5.

3.3 Optical properties

It is well known that the Tb^{3+}-doped phosphors are green light emitters. The photoluminescence excitation (PLE) spectrum of $Na_3Y_{0.96}Tb_{0.04}(PO_4)_2$ nanophosphor recorded at an emission wavelength (λ_{em}) of 545 nm is shown in Fig. 6. The spectrum depicts that there is a weak excitation peak at 272 nm corresponds to the transition $^7F_6 \rightarrow 5d$ and a sharp peak appears at 374 nm corresponds to the transition $^7F_6 \rightarrow {}^5D_3$ [1, 38]. The excitation wavelength of the most intense peak, i.e., 374 nm is selected to record the emission spectra under λ_{ex} = 374 with different dopant ions concentrations in $Na_3Y_{(1-x)}Tb_x(PO_4)_2$ (x = 0.015–0.06 mol) nanophosphors samples is shown in Fig. 7. The most intense peak in the emission spectra is at 545 nm. It contains numerous major peaks in the region of 400–650 nm. The region between 400 and 480 nm is assigned to blue emission and 480–650 nm region is considered as green emission. Peaks that lie between 400 and 480 nm mainly appear at 418 nm and 436 nm which correspond to $^5D_3 \rightarrow {}^7F_J$ (J = 5, 4) transition, respectively [39, 40]. Blue color of these nanophosphors is primarily due to these transitions. The emission peaks occurring at 488 nm, 545 nm and 583 nm correspond to transitions $^5D_4 \rightarrow {}^7F_J$ (J = 6, 5 and 4), respectively,

Table 2 Crystal size, dislocation density, and strain parameters of $Na_3Y_{(1-x)}Tb_x(PO4)_2$ (x = 0.015–0.06 mol) nanophosphors

Sr. No.	Tb^{3+} concentration (mol)	FWHM (β) (degree)	D (nm)	δ (10^{-4} nm^{-2})	ε (strain)
1.	0.015	0.25	34.7	8.30	0.0036
2.	0.025	0.27	32.1	9.7	0.0039
3.	0.035	0.27	32.16	9.6	0.0039
4.	0.04	0.29	32.14	9.68	0.0041
5.	0.05	0.28	30.99	10.41	0.0040
6.	0.06	0.30	28.9	11.97	0.0043

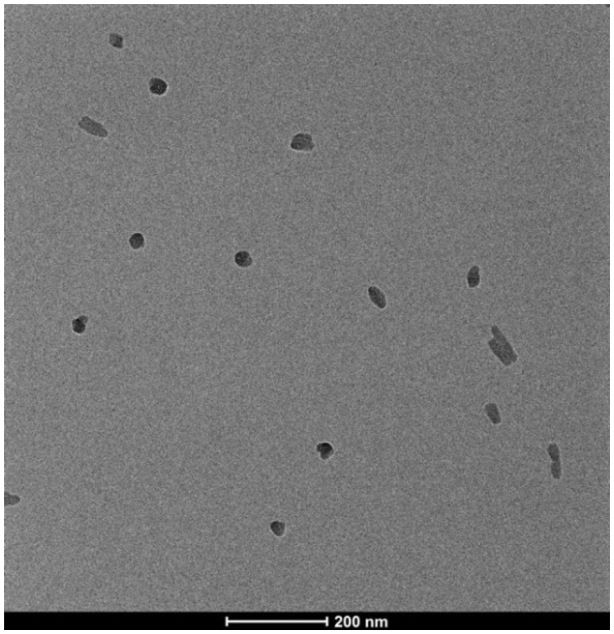

Fig. 4 TEM micrograph of $Na_3Y_{0.96}Tb_{0.04}(PO_4)_2$ nanophosphor

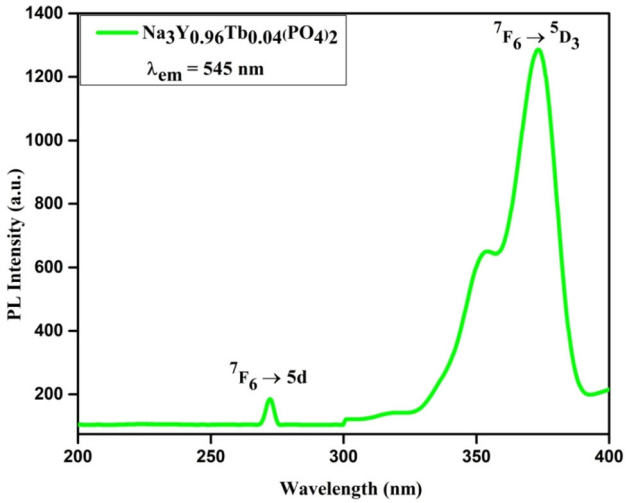

Fig. 6 Photoluminescence excitation spectrum of $Na_3Y_{0.96}Tb_{0.04}(PO_4)_2$ nanophosphor at λ_{em} = 545 nm

responsible for the green color of nanophosphors [41, 42]. With the increase in the concentration of Tb^{3+} ions, emission color shifts from light blue to light green color. This color tunability may be due to the cross-relaxation phenomenon. The cross-relaxation phenomenon occurs due to the same energy gap between excited state $^5D_3 \rightarrow {}^5D_4$ and ground state $^7F_6 \rightarrow {}^7F_0$ levels as shown in the schematic energy transfer diagram in Fig. 8 [42, 43]. As the concentration of Tb^{3+} ions increases, peaks intensity increases up to the concentration x = 0.04

Fig. 5 EDX image of $Na_3Y_{0.96}Tb_{0.04}(PO4)_2$ nanophosphor

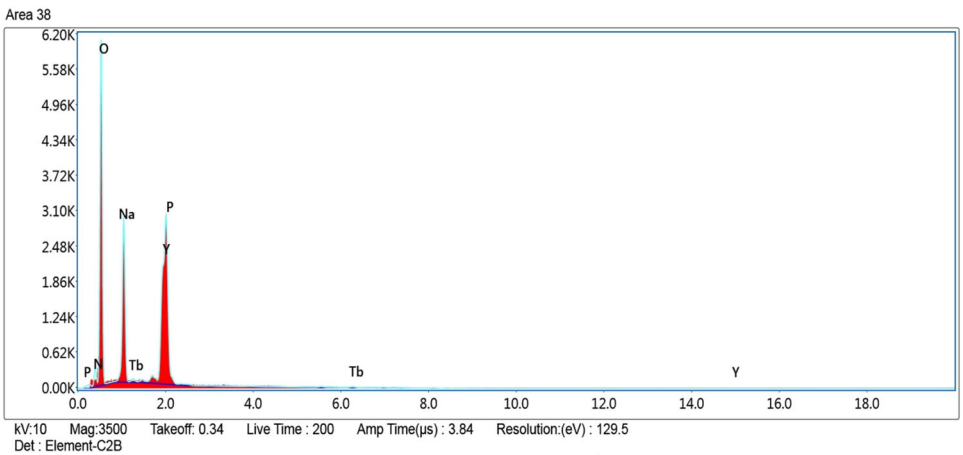

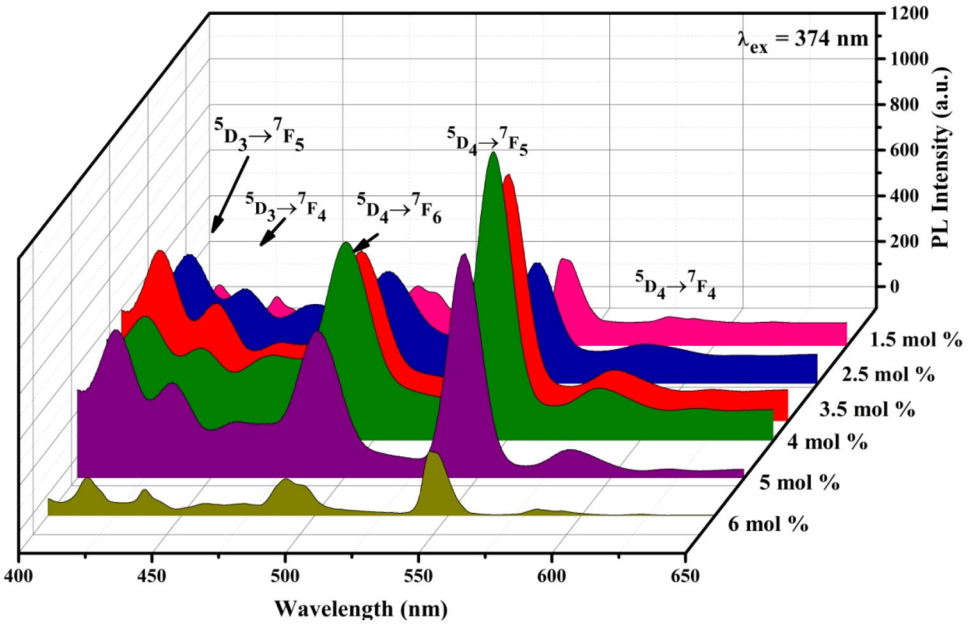

Fig. 7 PL emission spectra of $Na_3Y_{1-x}Tb_x(PO_4)_2$ (x = 0.015–0.06 mol) nanophosphors studied at λ_{ex} = 374 nm

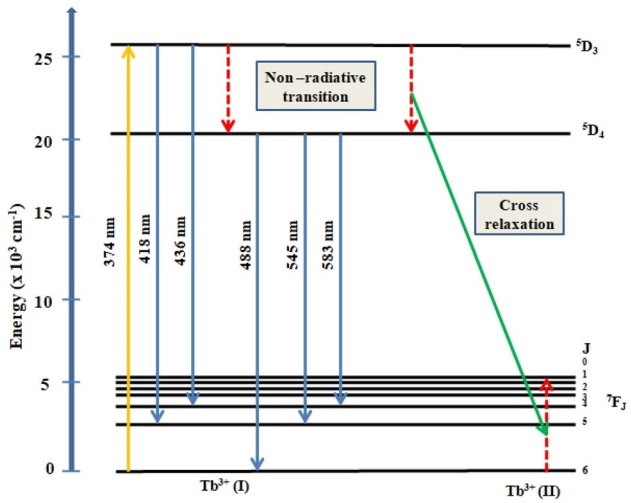

Fig. 8 Schematic energy transfer mechanism in Tb^{3+} ions for $Na_3Y(PO_4)_2$:Tb^{3+} nanophosphors

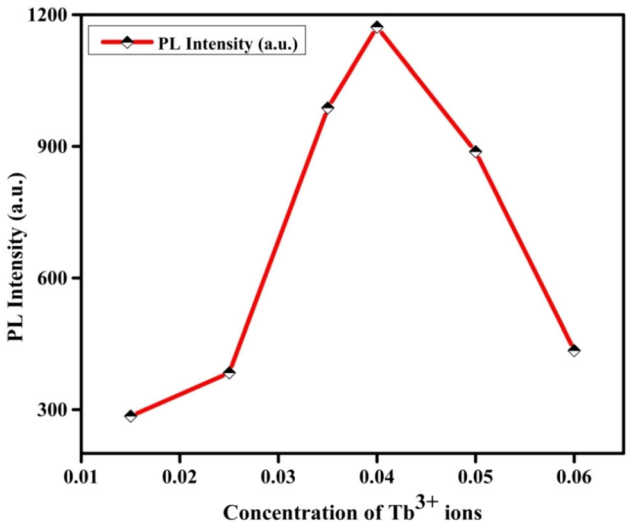

Fig. 9 Variation of the emission intensity as a function of Tb^{3+} concentration in $Na_3Y_{1-x}Tb_x(PO_4)_2$ (x = 0.015–0.06 mol) nanophosphors

(4 mol %), and after that intensity decreases as shown in Fig. 9. This decrease in intensity may be due to the concentration quenching arising from over doping of dopant ions and an increase in non-radiative energy transfer [14, 44].

The energy transfer mechanism occurring through the radiative and non-radiative pathway is depicted in Fig. 8. Generally, the mechanism responsible for the concentration quenching occurs via three ways, i.e., electric multipolar interactions, exchange interactions, and radiations re-absorption [45]. The probability of radiation re-absorption is excluded as there is no coinciding occurs between excitation and emission spectra [46]. The mechanism which is responsible for concentration quenching can be further determined by calculating the critical distance (R_c) using the following equation [45]:

$$R_c = 2\left[\frac{3V}{4\Pi N x_c}\right]^{\frac{1}{3}} \quad (5)$$

where V is volume of the unit cell, N represents the number of replaceable cations in the unit cell and x_c

represents critical concentration beyond that intensity decreases. By substituting $V = 1354.63$ (Å^3), N = 8, and $x_c = 0.04$ in the above-mentioned mathematical expression, the value of R_c comes out to be nearly 21 Å. If R_c value comes out to be less than 5 Å then the mechanism may be radiation absorption or exchange interionic or if R_c value comes out to be greater than 5 Å then the mechanism may be multipole interaction [47, 48]. Our R_c value is much greater than 5 Å, hence the possibility of exchange interactions is eliminated which means electric multipole–multipole interactions is responsible for concentration quenching phenomenon. By applying the logarithmic form of Dexter's theory, a particular kind of multipole–multipole interactions can be determined by the following expression [14, 47]:

$$\log\left(\frac{I}{x}\right) = -\frac{Q}{3}\log x + A \tag{6}$$

where x stands for concentration of dopant ions greater than critical concentration, I is the integral intensity of emission, I/x is emission intensity per dopant ions, A is constant, and Q is multipolar interaction constant whose value equals to 6, 8, or 10 are assigned to dipole–dipole (d–d), dipole–quadrupole (q–d) and quadrupole–quadrupole (q–q) interactions, respectively. Figure 10 shows a plot between log I/x and log x which is a straight line graph whose value of slope comes out to be − 3.3571. So, the value of Q is nearer to 10 which indicates that (q–q) interactions are responsible for the non-radiative energy transfer mechanism in Tb^{3+}-doped $Na_3Y(PO_4)_2$ nanophosphors.

The lifetime decay curve of $Na_3Y_{(1-x)}Tb_x(PO_4)_2$ (where x = 0.015–0.05 mol) at λ_{ex} = 374 nm and λ_{em} = 545 nm is depicted in Fig. 11. All the lifetime curves follow first exponential decay which is determined by the following equation [49, 50]:

$$I = I_o e^{-\frac{t}{\tau}} \tag{7}$$

where τ stands for the decay time, I and I_O are luminescence intensities at time t and 0, respectively. The first exponential nature of the decay curve shows that the dopant ions are homogeneously spread in the host matrix [51]. The fluorescence decay time decreases with the increase of concentration of Tb^{3+} ions which is listed in Table 3.

Furthermore, Auzel's fitting function is used to estimate the number of phonons generated during the process of decaying of the emitting level of Tb^{3+} ions which is described by the following equation [51]:

$$\tau_c = \frac{\tau_R}{1 + \frac{c}{c_0}e^{-\frac{N}{3}}} \tag{8}$$

where τ_R corresponds to the intrinsic lifetime value, τ_c shows the total value of PL lifetime corresponds to concentration c, c_o is constant and N is the number of phonons. The value of N is found to be 12 from Auzel's fit function of experimental values of the lifetime which shows that the emitting level ($^5D_4$) is decayed by generating 12 phonons, whereas the

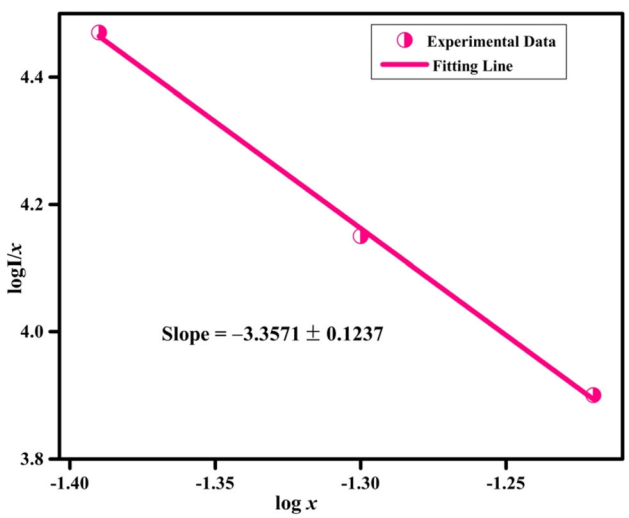

Fig. 10 Plot of log (I/x) as a function of log (x) in $Na_3Y(PO_4)_2$:Tb^{3+} nanophosphors

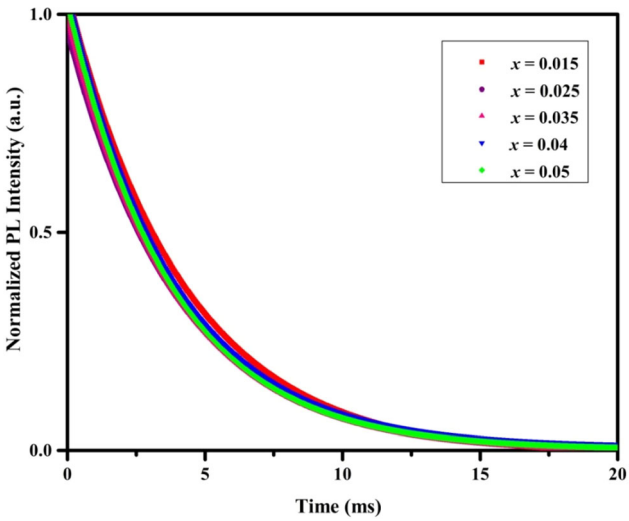

Fig. 11 Luminescence decay profile for the emission of $Na_3Y_{1-x}Tb_x(PO_4)_2$ (x = 0.015–0.05 mol) nanophosphors

Table 3 Photoluminescence life time, non-radiative rates, and quantum efficiencies of $Na_3Y_{1-x}Tb_x(PO_4)_2$ (x = 0.015–0.05 mol) nanophosphors

S. No.	Tb^{3+} concentration (mol)	Average life time (ms)	Non-radiative rates (s^{-1})	Quantum efficiency (%)
1.	0.015	3.94	5.67	97.76
2.	0.025	3.91	7.62	97.02
3.	0.035	3.88	10	96.02
4.	0.04	3.80	15	94.29
5.	0.05	3.78	16.40	93.79

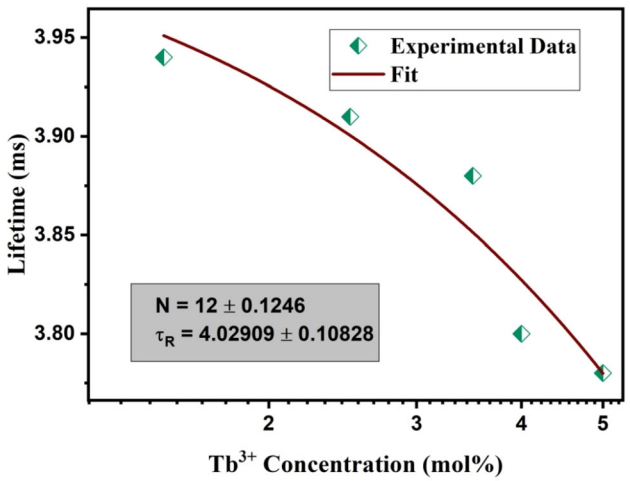

Fig. 12 Variation of photoluminescence lifetime with the doping concentration of Tb^{3+} ions using Auzel's function

value of intrinsic lifetime (τ_R) comes out to be 4.03 ms. A plot between the concentration of Tb^{3+} ions and decay lifetimes at different concentrations is presented in Fig. 12. Further, this τ_R value is used to determine quantum efficiency for the whole series with the help of the equation given below [52]:

$$\phi = \frac{\tau_o}{\tau_R} = \frac{A_R}{A_{R+A_{NR}}} \tag{9}$$

where A_R and A_{NR} show the radiative and non-radiative relaxation rate, respectively, while τ_o stands for an observed lifetime. Quantum efficiency and non-radiative rates for $Na_3Y_{1-x}Tb_x(PO_4)_2$ nanophosphors (where x = 0.015–0.05 mol) are also shown in Table 3.

To determine the colors emitted by the nanophosphors, the CIE chromaticity coordinates for the series of $Na_3Y_{1-x}Tb_x(PO_4)_2$ nanophosphors (where x = 0.015–0.05 mol) are calculated by employing the MATLAB software which is based upon the implementation of their relevant PL emission data.

Table 4 CIE1931 Color Coordinates for $Na_3Y_{1-x}Tb_x(PO_4)_2$ (x = 0.015–0.05 mol) nanophosphors

Sr. No.	Tb^{3+}concentration (mol)	Color coordinates (x, y)
1.	0.015	(0.210, 0.265)
2.	0.025	(0.221, 0.322)
3.	0.035	(0.222, 0.331)
4.	0.04	(0.221, 0.360)
5.	0.05	(0.240, 0.420)

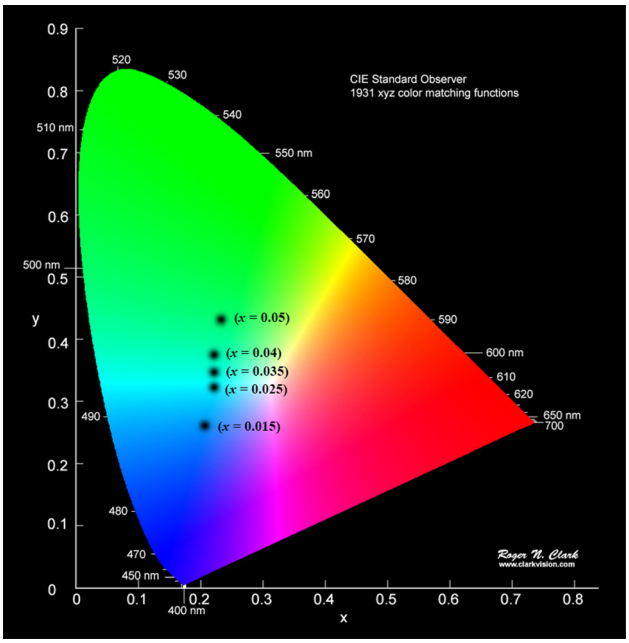

Fig. 13 CIE chromaticity diagram for different concentrations of Tb^{3+}-doped in $Na_3Y_{(1-x)}Tb_x(PO_4)_2$ nanophosphors

Calculated Color coordinates of whole series are displayed in Table 4; Fig. 13 represents the CIE 1931 chromaticity diagram for the same. All the CIE coordinates lie in light bluish to the greenish region which further proves the color tunability from blue to

green emission with changing concentration of Tb^{3+} ions. Hence, these nanophosphors show their potential utility for WLEDs as blue-green components in near-UV-based WLEDs and in solid-state lighting.

4 Conclusion

The solution combustion method was used to synthesize a series of Tb^{3+}-doped $Na_3Y(PO_4)_2$ nanophosphors. Various structural and photoluminescent characteristics of synthesized phosphors were analyzed using different techniques such as XRD, TEM, PL, and CIE chromaticity analysis. XRD results showed that the resulting phosphor $Na_3Y_{0.96}Tb_{0.04}(PO_4)_2$ has an orthorhombic crystal structure with space group Pca21(29). The emission spectrum of the whole series recorded at λ_{ex} = 374 nm showed the presence of two main peaks at 545 nm and 480. The value of R_c came out to be 21 which lastly concluded the existence of multipole–multipole interactions among Tb^{3+} ions. PL results showed that intensity increased with an increase in the concentration of the dopant Tb^{3+} ions up to $x = 0.04$ (4 mol%) and after that intensity decreased with an increase in the concentration of the dopant ions due to concentration quenching effect. Upon employing Auzel's fitting function, intrinsic radiative lifetime (4.03 ms) and quantum efficiency (94.29%) were also obtained for the $Na_3Y_{0.96}Tb_{0.04}(PO_4)_2$ nanophosphor. CIE color coordinates for nanophosphor of optimum concentration were found to be (0.221, 0.36) and there was color tunability from light blue to green with the increase in the concentration of dopant Tb^{3+} ions. High quantum efficiency and dependence of chromatic behavior on concentration suggest that these nanophosphors might have some potential utility in RGB phosphor-based WLEDs using NUV excitation and in display gadgets.

Acknowledgements

One of the authors, Manju Dahiya is thankful for financial help in the form of a senior research fellowship from the Council of Scientific and Industrial Research, India (CSIR), New Delhi, India (Award No. 09/1063/0014/2017-EMR-I).

References

1. X. Li, Y. Zhang, D. Geng, J. Lian, G. Zhang, Z. Hou, J. Lin, J. Mater. Chem. C **2**, 9924 (2014)
2. R.G. Nair, S. Nigam, V. Sudarsan, R.K. Vatsa, V.K. Jain, J. Lumin. **195**, 271 (2018)
3 M. Dalal, V.B. Taxak, S. Chahar, J. Dalal, A. Khatkar, S.P. Khatkar, J. Alloys Compd. **686**, 366–378 (2016)
4. C. Pratapkumar, S.C. Prashantha, H. Nagabhushana, M.R. Anilkumar, C.R. Ravikumar, H.P. Nagaswarupa, D.M. Jnaneshwara, J. Alloys Compd. **728**, 1124 (2017)
5. K.N. Venkatachalaiah, H. Nagabhushana, G.P. Darshan, R.B. Basavaraj, B. Daruka, Prasad, S.C. Sharma, Spectrochim. Acta - Part A Mol. Biomol. Spectrosc. **184**, 89 (2017)
6. S. Ashwini, S.C. Prashantha, R. Naik, Y.V. Naik, H. Nagabhushana, D.M. Jnaneshwara, Optik (Stuttg). **192**, 162956 (2019)
7. T. Senden, E.J. van Harten, A. Meijerink, J. Lumin. **194**, 131 (2018)
8. Y. Chen, K. Wai Cheah, M. Gong, J. Lumin. **131**, 1589 (2011)
9. Z. Yang, X. Li, Y. Yang, X. Li, J. Lumin. **122–123**, 707 (2007)
10. H. Jiao, Q. Ma, L. He, Z. Liu, Q. Wu, Powder Technol. **198**, 229 (2010)
11. X. Zeng, S.J. Im, S.H. Jang, Y.M. Kim, H. Bin Park, S.H. Son, H. Hatanaka, G.Y. Kim, S.G. Kim, J. Lumin. **121**, 1 (2006)
12. A. Jose, M. Ocan, J. Garc, E. Cantelar, and A. I. Becerro, (2014)
13. N. Hirosaki, R.J. Xie, K. Kimoto, T. Sekiguchi, Y. Yamamoto, T. Suehiro, M. Mitomo, Appl. Phys. Lett. **86**, 1 (2005)
14. X. Huang, B. Li, H. Guo, J. Alloys Compd. **695**, 2773 (2017)
15. C.C. Lin, R.S. Liu, J. Phys. Chem. Lett. **2**, 1268 (2011)
16. M. Kloss, B. Finke, L. Schwarz, D. Haberland, J. Lumin. **72–74**, 684 (1997)
17. T. Aitasalo, M. Guzik, W. Szuszkiewicz, J. Hölsä, B. Keller, J. Legendziewicz, J. Alloys Compd. **380**, 405 (2004)
18. M. Guzik, T. Aitasalo, W. Szuszkiewicz, J. Hölsä, B. Keller, J. Legendziewicz, J. Alloys Compd. **380**, 368 (2004)
19. D.P. Dutta, A.K. Tyagi, Solid State Phenom. **155**, 113 (2009)
20. S. Khosravi Ghandomani, B. Khoshnevisan, R. Yousefi, J. Mater. Sci. Mater. Electron. **29**, 18989 (2018)
21. N. Alonizan, S. Rabaoui, K. Omri, R. Qindeel, Appl. Phys. A Mater. Sci. Process. **124**, 1 (2018)
22. G.S. Rama Raju, E. Pavitra, G. Nagaraju, X.Y. Guan, J.S. Yu, RSC Adv. **5**, 22217 (2015)
23 J. Dalal, M. Dalal, S. Devi, A. Hooda, A. Khatkar, R.K. Malik, V.B. Taxak, S.P. Khatkar, J. Mater. Sci. Mater. Electron. **30**, 17547–17558 (2019)

24. J. Thakur, D.P. Dutta, H. Bagla, A.K. Tyagi, J. Am. Ceram. Soc. **95**, 696 (2012)
25. A. Podhorodecki, M. Nyk, J. Misiewicz, W. Strek, J. Lumin. **126**, 219 (2007)
26. S. Mahlik, E. Cavalli, M. Amer, P. Boutinaud, Phys. Chem. Chem. Phys. **17**, 32341 (2015)
27 D.P. Dutta, R.S. Ningthoujam, A.K. Tyagi, AIP Adv. **2**, 5 (2012)
28 T. Grzyb, R.J. Wiglusz, A. Gruszeczka, S. Lis, Dalton Trans. **43**, 17255 (2014)
29 A. Matraszek, I. Szczygieł, B. Szczygieł, J. Alloys Compd. **612**, 411 (2014)
30 S.T. Aruna, *Solution Combustion Synthesis* (Elsevier Inc, Amsterdam, 2017).
31. S.T. Aruna, A.S. Mukasyan, Curr. Opin. Solid State Mater. Sci. **12**, 44 (2008)
32. K. Li, H. Lian, M. Shang, J. Lin, Dalt. Trans. **44**, 20542 (2015)
33. R. Zsigmondy, P. Scherrer, Kolloidchem. Ein Lehrb. **277**, 387 (1912)
34. A.L. Patterson, Phys. Rev. **56**, 978 (1939)
35. G. Will, N. Masciocchi, W. Parrish, M. Hart, J. Appl. Crystallogr. **20**, 394 (1987)
36. A. Chowdhury, B. Biswas, M. Majumder, M.K. Sanyal, B. Mallik, Thin Solid Films **520**, 6695 (2012)
37. E. Pavitra, G.S.R. Raju, Y.H. Ko, J.S. Yu, Phys. Chem. Chem. Phys. **14**, 11296 (2012)
38. A. Raja, G. Annadurai, D.Joseph Daniel, P. Ramasamy, J. Alloys Compd. **683**, 654 (2016)
39. D. Kumar, M. Sharma, D. Haranath, O.P. Pandey, J. Alloys Compd. **695**, 726 (2017)
40. H. Dahiya, M. Dalal, A. Siwach, M. Dahiya, V.B. Taxak, S.P. Khatkar, D. Kumar, J. Mater. Sci. Mater. Electron. **31**, 3750 (2020)
41. H. Dahiya, M. Dalal, J. Dalal, V.B. Taxak, S.P. Khatkar, D. Kumar, Mater. Res. Bull. **99**, 86 (2018)
42. H. Guo, B. Devakumar, B. Li, X. Huang, Dye. Pigment. **151**, 81 (2018)
43. X. Zhou, S. Jiang, G. Xiang, X. Tang, X. Luo, L. Li, X. Zhou, J. Am. Ceram. Soc. **101**, 3076 (2018)
44. L. Wang, L. Shi, N. Liao, H. Jia, P. Du, Z. Xi, L. Wang, D. Jin, Mater. Chem. Phys. **119**, 490 (2010)
45. G. Blasse, Phys. Lett. A **28**, 444 (1968)
46. X. Zhang, F. Zhou, J. Shi, M. Gong, Mater. Lett. **63**, 852 (2009)
47. D.L. Dexter, J.H. Schulman, J. Chem. Phys. **22**, 1063 (1954)
48. Y.C. Fang, X.R. Huang, Y.Der Juang, S.Y. Chu, J. Am. Ceram. Soc. **95**, 1613 (2012)
49. A. Prasad, A.S. Rao, M. Gupta, G.V. Prakash, Mater. Chem. Phys. **219**, 13 (2018)
50. M. Dalal, V.B. Taxak, J. Dalal, A. Khatkar, S. Chahar, R. Devi, S.P. Khatkar, J. Alloys Compd. **698**, 662 (2017)
51. S. Devi, A. Khatkar, V.B. Taxak, M. Dalal, S. Chahar, J. Dalal, S.P. Khatkar, J. Alloys Compd. **767**, 409 (2018)
52. F. Paquin, J. Rivnay, A. Salleo, N. Stingelin, C. Silva, J. Mater. Chem. C **3**, 10715 (2015)